Transportation Engineering 19 (2025) 100310

Contents lists available at ScienceDirect

Transportation Engineering

journal homepage: www.sciencedirect.com/journal/transportation-engineering

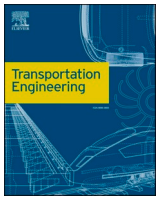

Full Length Article

Quantifying integrated safety risk in highly automated vehicles: A probabilistic approach to perception sensor uncertainty

Jinsil Lee [1], Mel Vincent Dela Cruz [1], Ralf Sturm [*]

Institute of Vehicle Concepts, DLR, Stuttgart, Germany

ARTICLE INFO

Keywords:
Autonomous vehicle
Integrated safety
Sensor uncertainty
Probabilistic
Perception

ABSTRACT

Introduction: Highly automated vehicles (AVs) rely on sensor data for target tracking and maintaining a safe separation distance during safety-critical operations such as forward collision avoidance. However, the inherent uncertainty in perception sensor measurements can lead to inaccurate tracking, which poses challenges for ensuring passenger safety. Method: This study proposes a method to quantify integrated safety risk using a probabilistic approach, incorporating various scenarios of perception sensor uncertainty and linking them to corresponding collision risks and subsequent serious passenger injury risks. A novel approach in this method involves subdividing the risk for each distance to the target, as defined by a perception uncertainty model. These risks are then integrated to compute the total safety of the ego-vehicle's passengers. Results and conclusions: By considering both target presence and absence hypotheses, the algorithm innovatively addresses risks posed by potentially undetected targets, significantly enhancing user protection and advancing AV safety. Practical Applications: The developed algorithm contributes to the integrated safety of AVs by offering guidance on regulating a minimum separation distance or maximum vehicle speed for a given vehicle sensor set, or specifying the sensor specifications that should be equipped on a vehicle. This approach aims to enhance the reliability and safety of automated driving systems, ensuring a higher standard of passenger safety and fostering trust in automated vehicle technologies.

1. Introduction

Automated vehicles (AVs) have the potential to significantly enhance the availability, safety, and efficiency of future mobility. The Society of Automotive Engineers (SAE) defines six levels of automation, ranging from Level 0 (no automation) to Level 5 (full automation) [39]. Continuous advancements in the automotive industry have led to the commercial availability of vehicles with driver assistance systems meeting SAE Level 3 standards. For instance, Mercedes-Benz's DRIVE PILOT system has received Level 3 certification in the U.S., initially approved in Nevada, marking significant milestones toward higher levels of autonomy [30]. Level 3 (conditional automation) systems can manage driving tasks independently under specific conditions but require driver intervention when requested.

While Level 3 systems are becoming available, engineers are now focusing on deploying AVs with higher levels of automation on public roads. Level 4 systems perform all driving tasks without driver supervision under specific conditions, while Level 5 systems are capable of full automation in all conditions, necessitating stringent safety regulations. An example of Level 4 technology is Waymo's autonomous ride-hailing service, which operates without human driver input in specific areas but is still undergoing broader testing and regulatory approval [23]. Ensuring system safety remains a major industry concern, essential for advancing automation and deploying these technologies on public roads [34].

While human drivers leverage sensory perception and their accumulated driving experiences, AVs rely on perception sensors such as lidar, radar, and cameras, and their software algorithms. [31,44,47]. Perception sensors in AVs, along with their processing algorithms, provide information on the existence, distance, direction, and type of targets. AVs utilize this sensor information during their operation. This can include safety-critical functions such as forward collision avoidance (FCA), lane change assistance (LCA), and adaptive cruise control (ACC) for vehicles with lower levels of automation, or the entire dynamic driving task (DDT) for Level 3 or higher automation [46]. However, these sensors are not perfect and include uncertainties, which become

* Corresponding author.
E-mail address: Ralf.Sturm@dlr.de (R. Sturm).
[1] First authors. J. Lee and M. V. Dela Cruz are equally contributed.

https://doi.org/10.1016/j.treng.2025.100310
Received 2 October 2024; Received in revised form 17 February 2025; Accepted 20 February 2025
Available online 21 February 2025

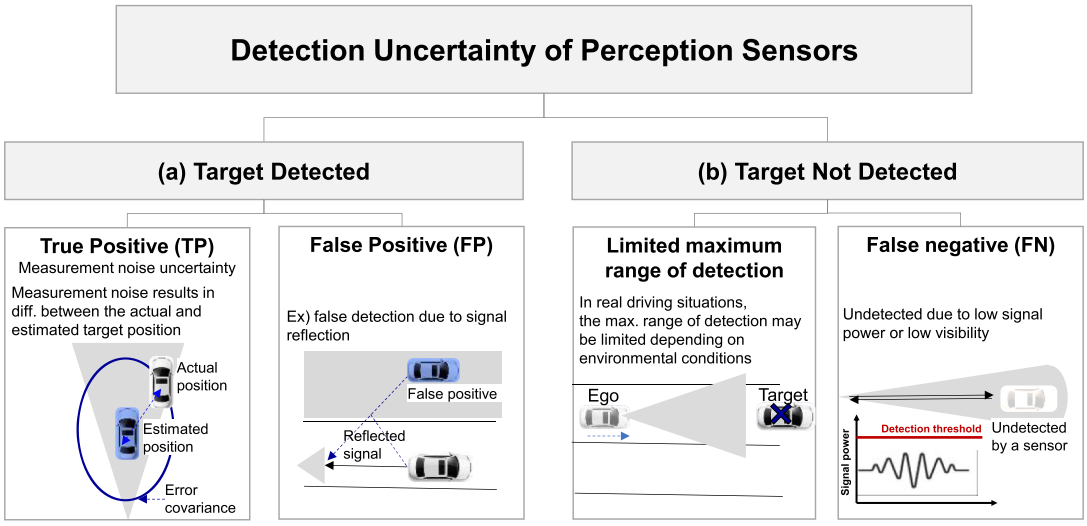

Fig. 1. The fault tree for detection uncertainty of perception sensors used in estimating the distance to a target and the target's speed.

more critical in highly automated, safety-critical applications. Potential uncertainties include nominal sensor noise, reduced detectable range due to the operational environment, false negatives due to low signal power, and false positives due to signal reflections [1,2,6]. Studies have investigated different perception sensors and their uncertainties [1,2,6,19,29,32,48]. These include review papers on perception sensors and types of uncertainties [6,29,44,48], as well as studies on methods for assessing the level of uncertainties [1,2,19,32]. For example, one study investigated the error level in the relative position on the highway when using a radar sensor and demonstrated an error of less than 1.5 m 75 % of the time in the longitudinal direction [32].

In order for AVs to take over the role of human drivers amidst the uncertainties of AV sensors, they must ensure the required level of driving safety based on current sensor sets and operational scenarios. Extensive efforts and studies to evaluate AV driving safety have been conducted using various approaches. One common approach by many companies is experimental evaluation by driving a vehicle equipped with a sensor set in an actual driving environment [23,42]. For example, Waymo has driven over 7.14 million fully autonomous miles as of October 2023, primarily in cities like Phoenix, San Francisco, and Los Angeles [23]. This extensive mileage has allowed Waymo to gather substantial data contributing to evaluations of AV safety and performance. Their research shows an 85 % reduction in crash rates involving any injury and a 57 % reduction in police-reported crash rates compared to human benchmarks. While this approach is essential for safety assurance, achieving a high level of safety with an experimental approach alone is a significant challenge and insufficient. Additionally, it is impractical to cover all operational conditions and sensor configurations through this approach alone; for example, when the sensor set changes, these experiments must be repeated.

Analytical evaluation of safety risk is a crucial approach in safety-critical applications. This method quantitatively assesses safety risks by employing mathematical models and assumptions about contributing factors, and then analyzing their impact on system safety. Civil aviation systems exemplify the use of analytical evaluation in both the design and assessment of system safety [15,24,25,37,38]. The target level of safety (TLS), established by the International Civil Aviation Organization (ICAO), specifies an acceptable level of safety for each flight operation. The calculated risk is then compared to the TLS to determine system viability. For instance, a TLS of 2.5×10^{-9} fatal accidents per aircraft flight hour is set for the loss of vertical separation [16].

Many experts argue that the safety requirements for sensors used in AVs must be defined to a high level, comparable to those of civil aviation, as their potential risk directly affects severe human injury or fatality [5,11,33,35,40]. Studies leveraging the analytical evaluation approach from civil aviation for AV applications are being conducted. These include suggesting navigation sensor requirements for AVs, such as GNSS-based localization [33,35], and Lidar-based localization [20]. For perception sensors, a study in [1] developed a method for perception reliability analysis to ensure AV safety and derived sensor reliability requirements analytically, given a TLS for perception. The above studies primarily focus on analyzing the reliability of the sensor itself rather than integrated safety, which considers the risk of severe injury and fatality of AV users associated with sensor uncertainty.

On the other hand, studies have considered the risk in terms of AV operational perspectives by proposing methods for computing the separation distance for AVs [28,36,41], which is a similar concept to vertical separation in civil aviation. For example, the company Mobileye proposed a mathematical model for a safe distance between vehicles known as responsibility-sensitive safety (RSS) [41]. This model is a function of the velocities, braking decelerations, and response times of both the ego and target vehicle. However, the separation distance is currently static and does not account for the uncertainties in the braking capabilities of different vehicles in adverse weather conditions. [10] propose a dynamic safety boundary for separation distance. Additionally, the separation distances proposed in [28,36,41] are primarily designed to avoid collisions by considering a vehicle's dynamic features without fully accounting for potential sensor uncertainties that might affect major safety issues. Furthermore, [45] reviewed a number of surrogate safety measures (SSMs), each capable of assessing the risk around an AV in different ways. They concluded that no single SSM can be universally applied to all scenarios an AV may encounter. Additionally, none of the discussed SSMs account for the risks that may arise due to sensor uncertainties. Therefore, a study that comprehensively incorporates all possible sensor uncertainties when determining key variables for driving safety is required.

This study introduces a novel methodology to analytically quantify the integrated safety of AVs under perception sensor uncertainties. It comprehensively considers the risk sequence from sensor uncertainty and collision risk to resulting human injury, integrating both active and passive safety systems. Active safety systems are designed to prevent collisions, whereas passive safety systems mitigate the impacts of collisions. Integrated safety, therefore, deals with the interactive consequences of both systems working together. Distinct from previous studies, which mainly focused on predicting collision risks under specific conditions [8,12,14,21] or examining the impacts of physical sensor coverage [4] or a time-to-collision analysis for the development of autonomous emergency braking [26], this study emphasizes the

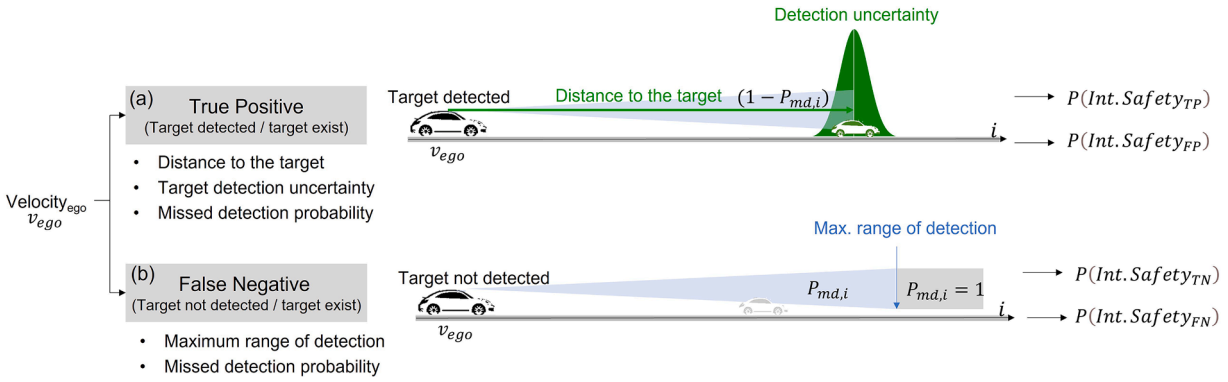

Fig. 2. Operational situations where (a) the target is detected, and (b) the target is not detected.

uncertainties in perception sensors and their impact on the final passenger risks. The methodology subdivides the risk for each potential distance to the target. This is done for each perception uncertainty hypothesis, which will be defined by the fault-tree of detection uncertainty in the following section. It accounts for varying passenger injury risks based on distance, corresponding collision risk, impact speed, and resulting human risks. Subsequently, all risks for each distance are integrated to determine the overall safety risk. In addition, by considering both the target presence and absence hypotheses, the algorithm addresses risks posed by potentially undetected targets, thereby enhancing user protection.

In Section 2, this study begins with a fault tree analysis, highlighting scenarios where a target is either detected or not detected by the vehicle's sensors. In the detection scenario, uncertainty arises due to sensor noise or signal reflection, leading to true positive (TP) and false positive (FP) detections, respectively. Conversely, in the non-detection scenario, the challenges include limited sensor range and false negatives (FN), influenced by factors like atmospheric attenuation and poor sensor visibility. The study then mathematically defines integrated safety risk under the defined hypotheses. In Section 3, simulations are conducted to demonstrate the risk calculations for TP and FN scenarios, showing the impact of parameters such as detection uncertainty, separation distance, vehicle speed, and sensor range. Sensitivity analyses indicate that safety risk increases with higher detection uncertainty and closer separation distances in TP scenarios, and with higher vehicle speeds and shorter detection ranges in FN scenarios. A demonstration for a use-case scenario of the suggested algorithm is shown using a Carmaker driving simulator, illustrating how the computed risk can be used to assure integrated safety during operation. Finally, Section 4 provides the conclusion of this study.

2. Definition of integrated safety under perception sensor uncertainty

2.1. Fault tree of detection uncertainties

In this section, a fault tree of detection uncertainty for perception sensors is structured as shown in Fig. 1, referring to extensive previous studies on perception sensor technologies for AVs [1,2,6,19,29,32,48]. Note that a fault tree is a tool used to identify potential sources of system failure. It is applied in analytical safety analysis and safety certification procedures for systems such as safety-critical aviation systems, which require a high level of safety [15,27,37].

The fault tree is divided into two scenarios: when a target is detected and when a target is not detected. The 'target detected' condition represents a scenario in which the ego-vehicle's sensor set detects a target, regardless of its actual presence. One hypothesis in this state is the true positive (TP), indicating the detection of an actually present target as shown in Fig. 1(a) (left). In this scenario, sensor measurement noise introduces uncertainty in estimating the target's distance and velocity. As shown in the figure, the estimated position of the vehicle (in blue) deviates from the actual position of the vehicle (in white). The level of uncertainty is represented by the error covariance. The level of uncertainty varies based on sensor quality, estimation algorithms, and environmental conditions. Another hypothesis in this state is the false positive (FP) as shown in Fig. 1(a) (right), which indicates the detection of a non-existent object, often caused by factors like signal reflection [1]. The figure illustrates this example, where an additional vehicle (in blue) is detected due to signal reflection from the original vehicle (in white).

Conversely, the 'target not detected' scenario is a situation where the ego-vehicle's sensor set indicates the absence of a target in front, regardless of its actual presence. Two hypotheses are considered in this state: the limited maximum range of detection (Fig. 1(b) (left)), also can also be referred to as the true negative (TN), and the false negative (FN) (Fig. 1(b) (right)). In practical operating environments, the specified ideal range of detection in sensor specifications may not be achievable due to environmental influences, such as harsh weather conditions. For instance, a radar sensor's detection range might be limited due to atmospheric attenuation [18]. Fig. 1(b) (left) illustrates this example, where the target is present but is not detected due to the limited detection range. Considering that atmospheric gases and rain contribute significantly to radio wave attenuation, a report on automotive radar sensors by the International Telecommunication Union (ITU) illustrates the relationship between attenuation and the detectable distance for a target due to rain and gas [18]. The report provides an example where the detectable distance to the vehicle is notably reduced from 100 m to 83.1 m (a 17 % reduction in range) when precipitation is at 50mm/h. It's important to note that a limited field of view of a perception sensor can also be a factor degrading detectability. Lastly, FN refers to a situation where tracking is not performed despite the presence of the target due to low signal power or poor sensor visibility [1], as illustrated in Fig. 1(b) (right). The fault hypotheses defined for each detection situation serve as the basis for the safety risk assessment in the next section.

2.2. Definition of integrated safety risk

In this section, the integrated safety risk is defined for both target-detected and target-non-detected scenarios using the following definitions:

D and *ND*: events representing target detection and target non-detection, respectively,

P and *NP*: events indicating target presence and absence, respectively,

C: event of collision between an ego-vehicle and a target,

R: event of human injury or fatality.

Fig. 2 provides an overview of four distinct scenarios and the parameters that will be employed to represent the resulting integrated safety probability. Fig. 2(a) illustrates the 'target detected' condition,

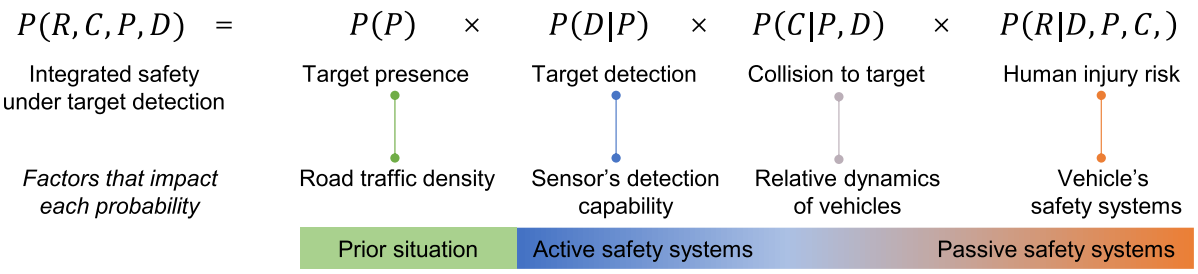

Fig. 3. The elements of integrated safety risk and factors that impact each probability.

while Fig. 2(b) represents the 'target not detected' condition. In both cases, the velocity of the ego-vehicle serves as a common input parameter. For the target detected scenario, key input parameters for the integrated safety evaluation include the distance to the target, target detection uncertainty, and missed detection probability of a sensor. As a result, the integrated safety risks associated with TP and FP hypotheses are evaluated, which are further discussed in the following section. In the target not detected scenario, as the target is not identified by the sensor, the distance to the target is no longer an applicable input parameter. Instead, the maximum detection range and the sensor's missed detection probability are used. The missed detection probability is assumed to be 1 beyond the sensor's maximum detection range, as shown in the figure. This scenario evaluates the safety risks associated with TN and FN hypotheses. Detailed definitions of the input parameters, fault hypotheses introduced in Fig. 2, and the methodology for their calculation, will be provided in the subsequent sections.

2.2.1. *The integrated safety risk under TP hypothesis* $P(Int.\ Safety_{TP})$

The integrated safety risk under the TP hypothesis can be defined as follows,

$$P(Int.\ Safety_{TP}) = P(R, C, P, D) \tag{1}$$

$P(Int.\ Safety_{TP})$ denotes the probability of integrated safety risk under the TP hypothesis. This is computed as the intersection of events the target detection (D), the target presence (P), the associated collision (C), and the resulting human risk (R). By the chain rule, Eq. (1) can be expressed as:

$$P(Int.\ Safety_{TP}) = P(R, C, P, D) = P(D)\cdot P(P|D)\cdot P(C|D, P)\cdot P(R|D, P, C) \tag{2}$$

Replacing the conditional probability $P(P|D) = P(D|P)\cdot P(P)/P(D)$, the above equation can be expressed as,

$$(Int.\ Safety_{TP}) = P(P)\cdot P(D|P)\cdot P(C|P, D)\cdot P(R|P, D, C) \tag{3}$$

Correspondingly, the probability of integrated safety can be expressed as the product of four probabilities. Fig. 3 illustrates these four components and the factors that influence each probability. Each probability will be discussed in detail in the following sections, with a brief introduction provided here.

The prior probability of target presence, $P(P)$, depends on road traffic

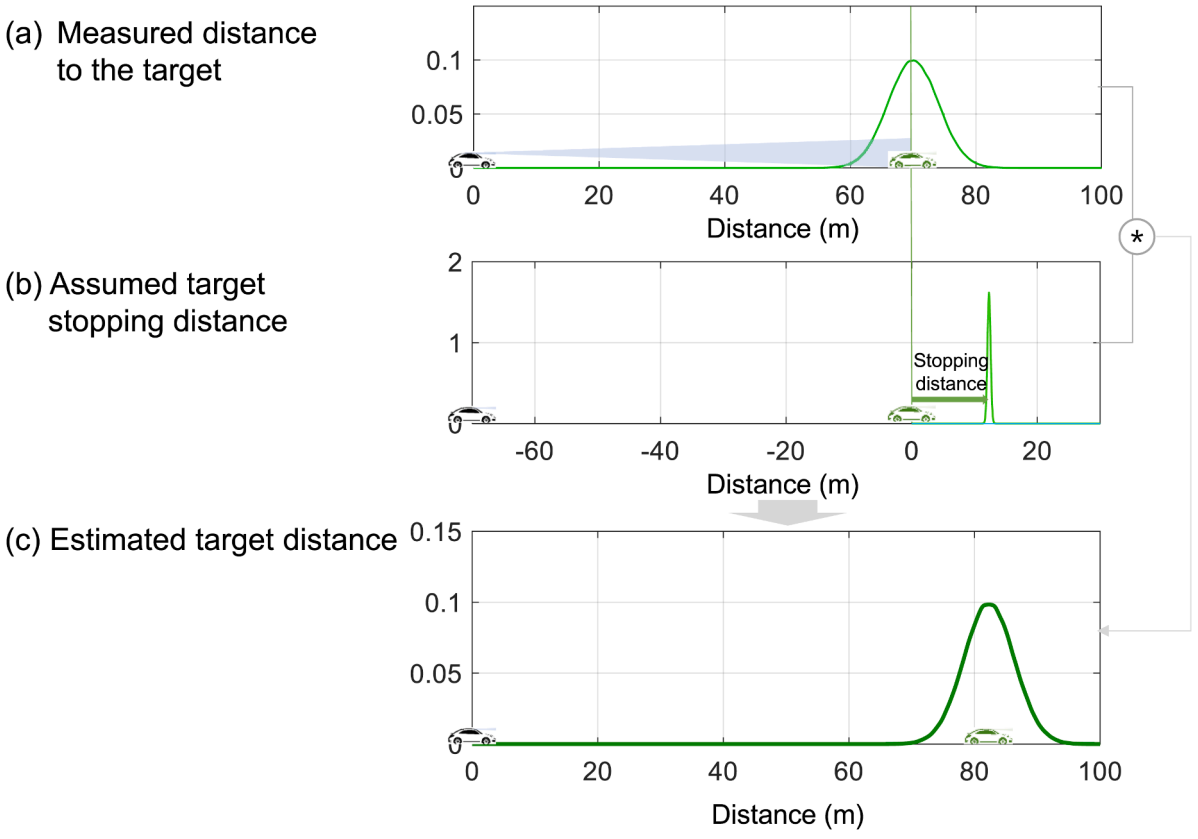

Fig. 4. Modeled distribution of the target distance.

situations. The detection probability given the target presence, $P(D|P)$, is affected by the sensor's detection capability. Given detection, the collision risk to the target, $P(C|P,D)$, is influenced by the relative dynamics of the vehicle. Lastly, the human injury risk given all the conditions, $P(R|P,D,C)$, depends on the vehicle's safety systems.

In this study, we define integrated safety as the comprehensive safety that encompasses both active and passive safety systems, given the driving situations. The prior probability, $P(P)$, represents the initial traffic scenario. The detection probability, $P(D|P)$, pertains to the active safety systems that detect a target prior to a collision. The collision risk, $P(C|P,D)$, is calculated for each situation involving uncertain target locations due to the sensor's detection capability. The human injury risk, $P(R|P,D,C)$, are governed by passive safety systems that mitigate the consequences of a collision. This framework considers the entire spectrum of risks, providing a novel approach to vehicular safety.

The following provides a description for each component in more detail.

$\boldsymbol{P(P_i)}$: $P(P)$ is the prior probability of actual target presence. Assuming an ego-vehicle confidently asserts the absence of a target (not based on sensor output but on the actual situation), the prior probability can be assumed to be 0. However, in most cases, except for driving in a restricted area, this assumption might not be applicable. External information, such as road traffic density, can be used to estimate the prior probability of the vehicle's presence. Nevertheless, a conservative assumption should be made when complete information is unavailable, such as $P(P)$=1.

In this study, we propose to address the probability of target presence at each possible distance from an ego-vehicle, denoted as i, where r_{max} is sensor's maximum detection range, as follows.

$$P(P) = \int_{i=0}^{r_{max}} P(P_i)di \tag{4}$$

This allows us to analyze and associate different risks based on the potential target location as will be discussed in this section. Thus, we can express the equation as follows,

$$P(Int.\ Safety_{TP}) = \int_{i=0}^{r_{max}} P(P_i)\cdot P(D|P_i)\cdot P(C|P_i,D)\cdot P(R|P_i,D,C)di \tag{5}$$

In a TP situation, a sensor set on ego-vehicle provides the prior probability of target presence for each distance i. Eq. (6) defines the target distance as the sum of the measured target distance, $d_{target.meas}$, and the stopping distance of the target, $d_{target.stop}$, as shown in Fig. 4.

$$\begin{aligned} d_{target} &= d_{target.meas} + d_{target.stop} \\ &= d_{target.meas} + \frac{{v_{target.meas}}^2}{2\cdot\mu_{fmax,target}\cdot g} \end{aligned} \tag{6}$$

The target stopping distance is calculated using the general equation of stopping distance for a vehicle as a function of the measured target velocity, $v_{target.meas}$, the maximum friction coefficient of the target, $\mu_{fmax,target}$, and gravitational acceleration, g. The reaction time of a target driver is disregarded, and the maximum friction coefficient of the target, $\mu_{fmax,target}$, is applied to introduce conservatism into the risk calculation for the target distance, ensuring the target stopping distance is minimized.

In this study, the sensor outputs for the target distance and the target velocity are assumed to follow a Gaussian distribution as shown in Eq. (7)

$$\begin{aligned} d_{target.meas} &\sim N\left(\mu_{d_{target.meas}}, {\sigma^2}_{d_{target.meas}}\right) \\ v_{target.meas} &\sim N\left(\mu_{v_{target.meas}}, {\sigma^2}_{v_{target.meas}}\right) \end{aligned} \tag{7}$$

where $\mu_{d_{target.meas}}$ and $\mu_{v_{target.meas}}$ are the means, and ${\sigma^2}_{d_{target.meas}}$ and ${\sigma^2}_{v_{target.meas}}$ are the variances of the measured target distance and measured target velocity, respectively. Then, $d_{target.meas}$ follows a normal distribution as illustrated in Fig. 4(a), while $d_{target.stop}$ follows a non-central chi-square distribution as depicted in Fig. 4(b). The probability density function (pdf) of d_{target}, denoted as $f_{d_{target}}$, can be derived through the convolution of the two pdf functions, $f_{d_{target.meas}}$ and $f_{d_{target.stop}}$ as shown in Eq. (8) and as also demonstrated in Fig. 4(c).

$$f_{d_{target}} = f_{d_{target.meas}} * f_{d_{target.stop}} \tag{8}$$

Finally, $P(P_i)$ can be obtained by evaluating the distribution, $f_{d_{target}}(i)$, as shown in Eq. (9).

$$P(P_i) = f_{d_{target}}(i) \tag{9}$$

$\boldsymbol{P(D|P_i)}$: This is the probability of target detection by sensor sets of an ego-vehicle given the target presence at i. It depends on sensor's detection capability under operational conditions. This can be expressed using the probability of detection (equivalently, one minus the probability of missed detection) of a sensor set, denoted as,

$$P(D|P_i) = 1 - P_{md,i} \tag{10}$$

Eq. (5) can be expressed as follows by applying (9) and (10):

$$P(Int.\ Safety_{TP}) = \int_{i=0}^{r_{max}} \left(1 - P_{md,i}\right)\cdot f_{d_{target}}(i)\cdot P(C|P_i,D)\cdot P(R|P_i,D,C)di \tag{11}$$

Various studies have investigated the missed detection probability of different types of sensor sets. These include analytical, experimental, and machine-learning based approaches. The primary focus of this paper is to provide a framework for evaluating the safety risk given these inputs for sensor capabilities. This paper assumes a linearly increasing missed detection probability as a function of the distance from the ego-vehicle to the target, over the range of maximum detection for a sensor set.

$$P_{md,i} = \frac{P_{md,max}}{r_{max}}\cdot i \tag{12}$$

$\boldsymbol{P(C|P_i,D)}$: This is the probability of collision given the target presence at i and the target detection. When events P_i and D occur, the ego-vehicle will decelerate, associating its judgement with the situation. Collision risk arises when the ego-vehicle stops at or beyond the actual target location i as shown in (13). Let the ego-vehicle stopping distance be noted as $d_{stop,ego}$.

$$P(C|P_i,D) = P\left(i \le d_{stop,ego} \middle| P_i, D\right) \tag{13}$$

Similar to the calculation of the target stopping distance in Eq. (6), the stopping distance of an ego-vehicle is calculated as the distance traveled from the time a driver decides to stop the vehicle to the time the vehicle comes to a complete stop. It depends on t_r and $\mu_{f,ego}$, for a given speed, v_{ego}. In this study, the reaction time, t_r, of the ego-vehicle is modeled as a deterministic value by taking the benefit of an automation system that is much less affected by factors that depend on each human driver, such as the driver's ability to react to situations. t_r of an automaton system can be determined depending on the algorithm's latency time for processing information. Previous studies investigated the reaction time of an autonomous vehicle to be in the order of 0.5 s when using perception sensors to recognize situations [7,22,43]. On the other hand, the friction coefficient, $\mu_{f,ego}$, cannot be modeled as a deterministic value as it is the concern of external environmental conditions (i.e., the uncertain road conditions). To take this into account, a friction coefficient, $\mu_{f,ego}$ is modeled as a Gaussian distribution based on previous investigations on the friction coefficient [3,13]. The model for a friction coefficient is shown in (15) where $\overline{\mu}_{f,ego}$ is the expectation of $\mu_{f,ego}$ and ${\sigma^2}_{\mu_{f,ego}}$ is the standard deviation of the distribution.

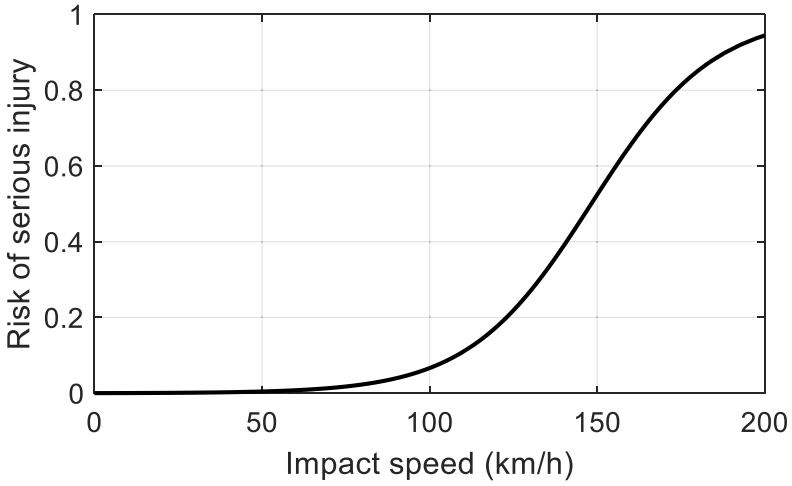

Fig. 5. The risk of human injury as a function of impact speed [9].

$$d_{stop,ego} = v_{ego}\cdot t_r + \frac{{v_{ego}}^2}{2\cdot\mu_{f,ego}\cdot g} \tag{14}$$

$$\mu_{f,ego} \sim N\left(\bar{\mu}_{f,ego}, {\sigma^2}_{\mu_{f,ego}}\right) \tag{15}$$

The distribution of the stopping distance of the ego-vehicle is obtained using a Monte Carlo simulation as illustrated in Fig. 6(a) in Section 3. We denote the pdf of the ego-vehicle's stopping distance as $f_{d_{stop,ego}}(j)$. The collision probability, given the pdf, can be expressed as the integration of the pdf over j-values that are greater than the target position i, as shown in (16), where j represents all possible stopping distances of the ego-vehicle.

$$P\left(C\middle|P_i, D, d_{stop,ego\,j}\right) = \int_{j=i}^{\infty} f_{d_{stop,ego}}(j)dj \tag{16}$$

Note that the collision occurs at a target location i, but the impact speed at i varies depending on the intended stopping distance of the ego-vehicle, j. For instance, if a vehicle has a shorter intended stopping distance, the impact speed at i would be lower. The impact speed will be reflected in the assessment of human injury risk.

$\boldsymbol{P}(\boldsymbol{R}|\boldsymbol{P_i}, \boldsymbol{D}, \boldsymbol{C})$: This is the probability of human injury risk due to the collision. This study considers human injury risk as injuries with a score of 3 or higher on the Abbreviated Injury Scale (AIS) severity score, noted as MAIS3+, which is classified as clinically serious injury [9], as well as fatal injuries. To compute the risk probability for each event, we employed the mathematical model on the relationship between impact speed and MAIS3+ and fatal injury risk, suggested in a previous study [9]. The study extensively investigated and analyzed a database obtained from an event data recorder (EDR) regarding crash data and formulated the relationship between impact speed and occupant injuries in different scenarios [9]. Eq. (17) presents the risk probability of a passenger for an ego-vehicle as a function of impact speed (v_{impact}) in a frontal collision scenario, as defined in [9]. Fig. 5 is a plot generated from the Eq. (17). Please note that the symbols and notation of formulas have been adapted to align with those used in this paper.

$$P(R|P_i, D, C) = \frac{1}{1 + e^{8.1231 - 0.0548\cdot v_{impact}}} \tag{17}$$

The impact speed, v_{impact}, is calculated with the friction coefficient of the ego-vehicle, $\mu_{f,ego\,j}$, assuming that the ego-vehicle stops at j. Concurrently, the collision occurs at i (where the target is) before reaching a complete stop, except in cases where i is the same as j. As stated previously, relative locations of the target position (i) and the ego-vehicle's stopping position (j) affect the impact velocity at i.

$$v_{impact,i} = \sqrt{{v_{ego}}^2 - 2\cdot\mu_{f,ego\,j}\cdot g\cdot\left(i - v_{ego}\cdot t_r\right)} \tag{18}$$

$$\mu_{f,ego\,j} = \frac{{v_{ego}}^2}{2g\cdot\left(j - v_{ego}\cdot t_r\right)} \tag{19}$$

By substituting (18) and (19) into (17), the risk probability is expressed as functions of i and j, as shown in (20).

$$P\left(R\middle|P_i, D, C, d_{stop,ego\,j}\right) = f_{risk}(i,j) = \frac{1}{1 + e^{8.1231 - 0.0548\cdot v_{ego}\sqrt{1-\left(i - v_{ego}\cdot t_r\right)/\left(j - v_{ego}\cdot t_r\right)}}} \tag{20}$$

Finally, the integrated safety probability under TP hypothesis is expressed as shown in (21).

$$P(Int.\ Safety_{TP}) = \int_{i=0}^{r_{max}} \left(1 - P_{md,i}\right)\cdot f_{d_{target}}(i) \int_{j=i}^{\infty} f_{d_{stop,ego}}(j)\ \cdot f_{risk}(i,j)djdi \tag{21}$$

2.2.3. *The integrated safety risk under FP hypothesis $P(Int.\ Safety_{FP})$*

In this study, the FP hypothesis is excluded from the computation of integrated safety risk, as we assume the potential collision probability under FP mode to be zero, given that the actual presence of a target is false. FP may cause the ego-vehicle to brake or maneuver unnecessarily, creating safety risks such as an increased likelihood of rear-end collisions if a following vehicle is too close or a loss of control in certain conditions (e.g., during harsh braking). While FP scenarios do carry potential risks, they often involve factors beyond the ego vehicle's control (e.g., the following vehicle's distance) or depend on vehicle-specific passive safety systems (e.g., smoother braking implementations). Since the primary focus of this study is to develop a framework for algorithms that compute integrated safety under sensor uncertainty, FP scenarios will be explored more thoroughly in future work, particularly in relation to their impact on the ego vehicle and overall system performance, with special attention to different in-vehicle passive safety systems.

2.2.3. *The integrated safety risk under FN hypothesis $P(Int.\ Safety_{FN})$*

In the FN case, sensors have a defined detection range but fails to detect the target due to factors such as low visibility or weak signals. To account for this, this paper assumes a uniform prior distribution of the target's presence within the sensor's maximum detection range when an FN occurs. This assumption influences the integration bounds for probability calculations, as a longer detection range increases the area over which the target's presence is considered, thereby affecting the overall safety risk assessment. Although the target's true location is

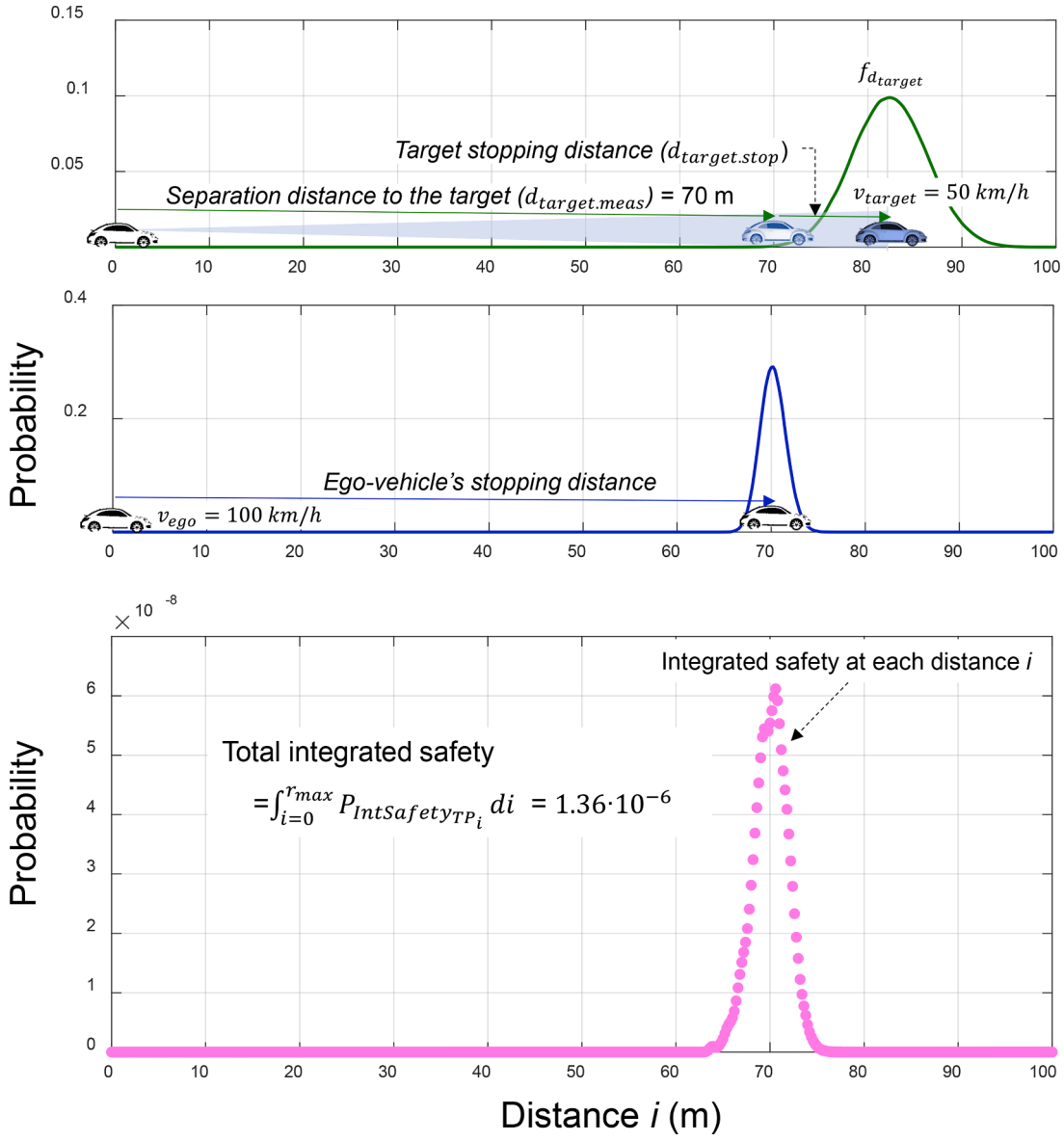

Fig. 6. Simulation of integrated safety risk in TP scenario.

independent of the sensor range, the risk quantification depends on the probabilistic constraints imposed by the detection range. As the sensor range increases, the probability of an undetected target being closer to the ego-vehicle decreases, which impacts the integrated safety risk calculation.

The integrated safety risk under the FN hypothesis can be defined as follows,

$$P(Int.\ Safety_{FN}) = P(R, C, P, ND) \tag{22}$$

This probability is calculated as the intersection of the events of non-detection (ND), target presence (P), associated collision (C), and the resultant human injury risk (R). Analogous to the TP case, Eq. (21) can be formulated as shown in Eq. (23).

$$P(Int.\ Safety_{FN}) = P(R, C, P, ND) = P(P) \cdot P(ND|P) \cdot P(C|ND, P) \cdot P(R|ND, P, C) \tag{23}$$

Each component is calculated using a distinct methodology compared to that of the TP hypothesis. This section presents each individual component, emphasizing their unique aspects.

$\boldsymbol{P}(\boldsymbol{P_i})$: In a target non-detection scenario, there is no external sensor data to provide the prior probability of target presence for each distance i from an ego-vehicle. This study assumes that a target is present within the range of the sensors and therefore considers a uniform distribution with a range from 0 to r_{max}, as follows:

$$P(P_i) = \frac{1}{r_{max}} \tag{24}$$

$\boldsymbol{P}(\boldsymbol{ND}|\boldsymbol{P_i})$: This is the probability of target non-detection by the sensor sets of an ego-vehicle, given the presence of the target. This can be expressed using the probability of missed detection as defined in (12).

$$P(ND|P_i) = P_{md,i} \tag{25}$$

$\boldsymbol{P}(\boldsymbol{C}|\boldsymbol{P_i}, \boldsymbol{ND})$: This represents the probability of a collision given the presence of the target, but detection has failed. As the ego-vehicle is unable to detect the target, it lacks the opportunity to decelerate properly. Consequently, the probability of a collision is influenced by the relative positions of the ego-vehicle and the target, and can thus be defined as follows:

$$P(C|P_i, ND) = H\left(j_{t_{eval}} - i\right) \tag{26}$$

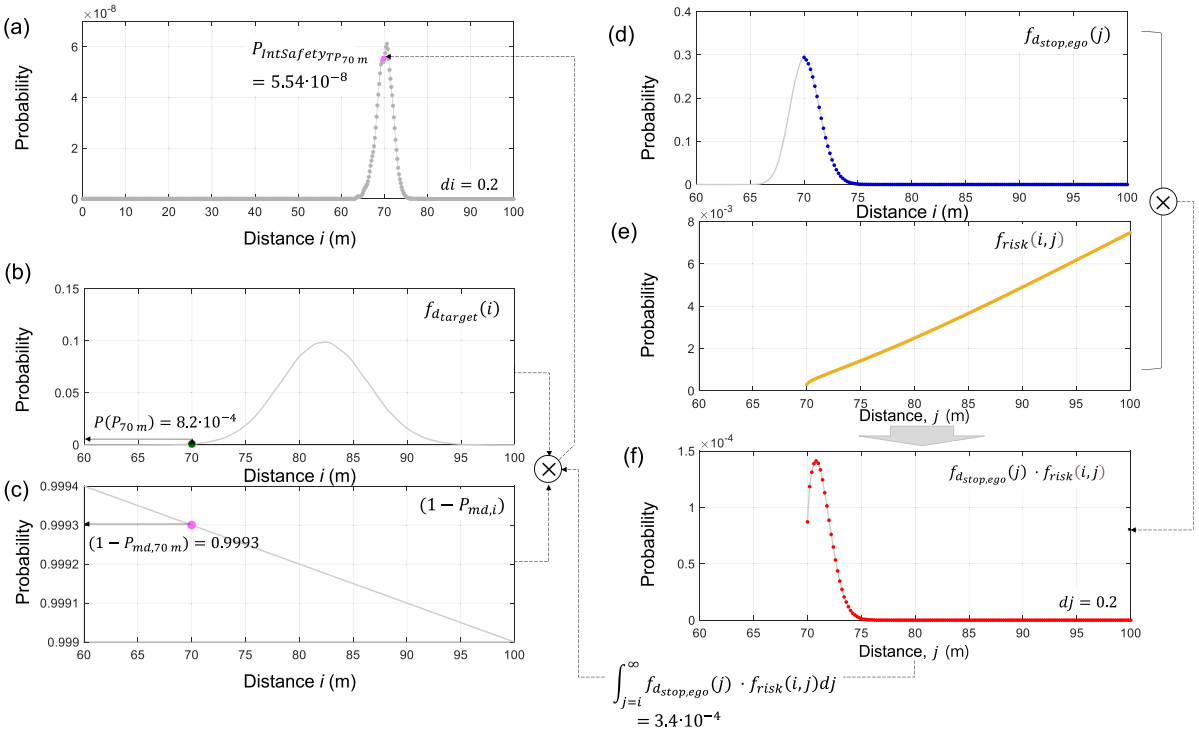

Fig. 7. Simulation of each element of integrated safety risk in TP scenario when i=70 m.

where $H(x)$ is the Heaviside step function, which returns 1 if x is positive and 0 otherwise. Let $j_{t_{eval}}$ represent the ego-vehicle's location after the risk evaluation interval (t_{eval}). For example, if the ego-vehicle conducts the risk calculation every 1 s, t_{eval} is 1 s. Eq. (26) yields a collision probability of 1 if the ego-vehicle will pass the target located at i after the evaluation time. This assumption is considered reasonable when t_{eval} is not too long, typically ranging from one to several seconds depending on the ego-vehicle's dynamics. Extending t_{eval} may change a situation during the calculation from a FN condition to a TP condition as the ego-vehicle advances and detects a previously unseen target. This shift can lead to a miscalculation of risk if the system continues to use the algorithm for FN situations when the TP algorithm should be applied.

$\boldsymbol{P}(\boldsymbol{R}|\boldsymbol{P_i}, \boldsymbol{ND}, \boldsymbol{C})$: The same mathematical equation introduced for the TP case applies to human injury risk, but the impact speed distinguishes the two cases. Since there is no indication for the ego-vehicle to decelerate, the ego-vehicle's impact speed depends on its speed at the point of collision at distance i, and it is generally higher than in the TP case. This speed could be the initial velocity (v_{ego}) or any other velocity depending on the ego-vehicle's maneuver. Let $v_{ego,i}$ denote the ego-vehicle's own velocity at distance i. Then, the human injury risk probability becomes as follows:

$$P(R|P_i, D, C) = \frac{1}{1 + e^{8.1231 - 0.0548 \cdot v_{ego,i}}} \tag{27}$$

The final expression for integrated safety under the FN hypothesis is as follows:

$$P(Int.\ Safety_{FN}) = \int_{i=0}^{r_{max}} P_{md,i} \cdot H\left(j_{t_{eval}} - i\right) \cdot \frac{1}{r_{max}} \cdot \frac{1}{1 + e^{8.1231 - 0.0548 \cdot v_{ego,i}}} di \tag{28}$$

2.2.4. The integrated safety risk under the limited range of detection hypothesis $P(Int.\ Safety_{TN})$

Under the limited range of detection hypothesis, the risk is defined when the ego-vehicle's driving path during the evaluation time exceeds the sensor's maximum range, r_{max}. This situation can be defined as a true negative (TN) situation due to the sensor's limitation. In this scenario, the most critical risk situation arises when the target is located just beyond r_{max}, making it undetectable by the sensor set. In this situation, the missed detection probability is set to 1, which distinctly differentiates it from a false negative (FN) scenario. Consequently, the missed detection probability the probability of target being present at r_{max}, and the corresponding collision probability are all set to 1. Additionally, the ego-vehicle's operating speed at r_{max} is applied to the human injury risk in Eq. (29). The final equation in this scenario is given in (29).

$$P(Int.\ Safety_{TN}) = 1 \cdot 1 \cdot 1 \cdot \frac{1}{1 + e^{8.1231 - 0.0548 \cdot v_{ego,r_{max}}}} \tag{29}$$

3. Simulations

Simulations for TP and FN scenarios were conducted under a forward collision avoidance (FCA) scenario to demonstrate the risk calculations using the developed Eqs. (21) and (28), respectively. Additionally, sensitivity analysis for significant parameters that affect each risk is also presented. For the simulations, an ego-vehicle equipped with a radar sensor and a target vehicle is assumed. While the algorithm can be extended to handle scenarios involving dynamic driving situations, multiple sensors, or interactions with multiple vehicles, this straightforward example is used to clearly illustrate the proposed algorithm.

3.1. . The integrated safety risk under TP hypothesis

Fig. 6 shows a simulation that presents the determination of integrated safety risk in the TP scenario. The Fig. 6(a) depicts the simulation scenario, with the ego-vehicle's velocity set at 100 km/h, while measuring the target speed at 50 km/h. The ego-vehicle is measuring the separation distance to the target as 70 m using the sensor. Fig. 6(a) and Fig. 6(b) show the estimated target position, $f_{d_{target}}$, in green, and the stopping distance of an ego-vehicle, $f_{d_{stop,ego}}$, in blue, respectively. Fig. 6(c) shows the risk at each potential target location i at the time of evaluation. The total integrated safety is the summation of all, resulting in $1.36{\bullet}10^{-6}$. The trend of risk as a function of i shows a dependency on the

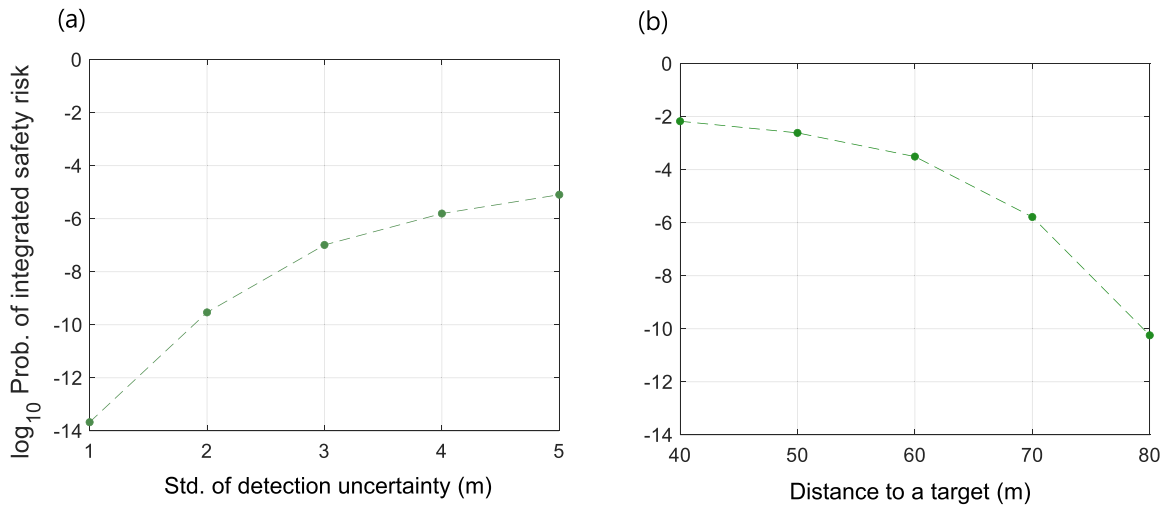

Fig. 8. Sensitivity analysis for TP scenarios as a function of the standard deviation of detection uncertainty (a) and the distance to a target (b).

ego-vehicle's stopping distance represented in blue. However, it can be observed that the overall distribution is skewed towards the right side due to the influence of the target's stopping distance, which has a higher mean value compared to the ego-vehicle's stopping distance.

Now, Fig. 7 focuses on the risk at i=70 m and provides detailed information on how the risk is calculated. The risk at $i = 70$ m is $5.54 \bullet 10^{-8}$, as shown in Fig. 7(a). This value is the product of the probability of true positive target presence at i, the probability of collision between the ego-vehicle and the target, and the probability of human injury. The probability of true positive target presence at i is evaluated by multiplying the prior probability of target location at i given by the sensor (Fig. 7(b)) and the probability of detection by the sensor (Fig. 7(c)). A collision between ego-vehicle and the target can occur when the ego-vehicle's stopping distance (j) is greater than i=70 m, as shown in blue (Fig. 7(d)). For each j, the human injury risk is calculated and shown in yellow (Fig. 7(e)). Note that the human injury risk increases as the ego-vehicle's stopping distance (j) increases due to the increased impact speed of the ego-vehicle when it reaches the target located at i=70 m. The injury risk is near zero at $j = i$, where the ego-vehicle stops at the target location without proceeding further. The integration over j of the values in Fig. 7 (f), which are the products of the risks in Fig. 7(d) and 7(e), shown in red, gives the human injury risk when a collision occurs at i, considering every possible ego-vehicle stopping distance j (and thus the different impact speeds at i). Multiplying this integration with the target detection probability at i=70 m and the prior probability of locations of the target gives the integrated safety risk of $5.54 \bullet 10^{-8}$, as shown in Fig. 7(a).

3.2. . Sensitivity analysis for TP scenario

The level of integrated safety risk varies depending on driving conditions. Sensitivity analysis is performed to provide a sense of the degree of risk change according to different parameters. Fig. 8 shows the sensitivity analysis of integrated safety for the target detection scenario, focusing on the standard deviations of detection uncertainty and the separation distances, which are key contributing parameters for safety. Fig. 8(a) illustrates the risk associated with sensors' detection uncertainty, where the standard deviation of the detection uncertainties ranges from 1 m to 5 m. It shows that the risk probability increases as the uncertainty increases. Fig. 8(b) depicts the probability of integrated safety risk for each separation distance, given fixed conditions for the other variables. It shows that the risk dramatically decreases at separation distances greater than 60 m. This sensitivity analysis can help determine the safe separation distance given a sensor set, or decide the appropriate quality of sensors to mount on a vehicle to ensure a level of safety.

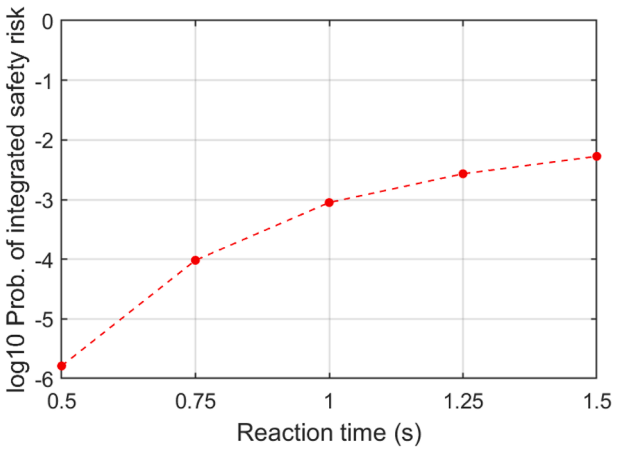

Fig. 9. Sensitivity analysis for TP scenarios as a function of reaction time.

It is also important to investigate the effects of reaction time, as it varies between vehicles. Fig. 9 presents a sensitivity analysis of integrated safety in TF scenarios as a function of reaction time, which ranges from 0.5 s to 1.5 s. The results indicate that risk increases with longer reaction times.

3.3. . The integrated safety risk under FN hypothesis

Fig. 10 shows a simulation illustrating the determination of integrated safety risk in the FN scenario. The ego-vehicle's velocity is set at 100 km/h, and the sensor's maximum range is 100 m. However, no target is detected by the sensor, leaving no prior information about the potential target location. The prior probability of the target location is assumed to follow a uniform distribution over the sensor's detection range, as shown in Fig. 10(a), which has a total sum of 1. By multiplying the missed detection probability (Fig. 10(b)) by the prior probability, we obtain the probability of the actual target presence at each distance i under the FN scenario.

As discussed in Section 2.2.3, a collision can occur up to the distance of the ego-vehicle's distance traveled before potential collision during its evaluation time. In this simulation, the distance is calculated as 27.78 m by multiplying the ego-vehicle's velocity by the evaluation time of 1 s, as shown in Fig. 10(c). The probability of human risk is then computed based on the impact speed at the evaluation time, as shown in Fig. 10(d). Since the target has not been detected, the ego-vehicle does not perform

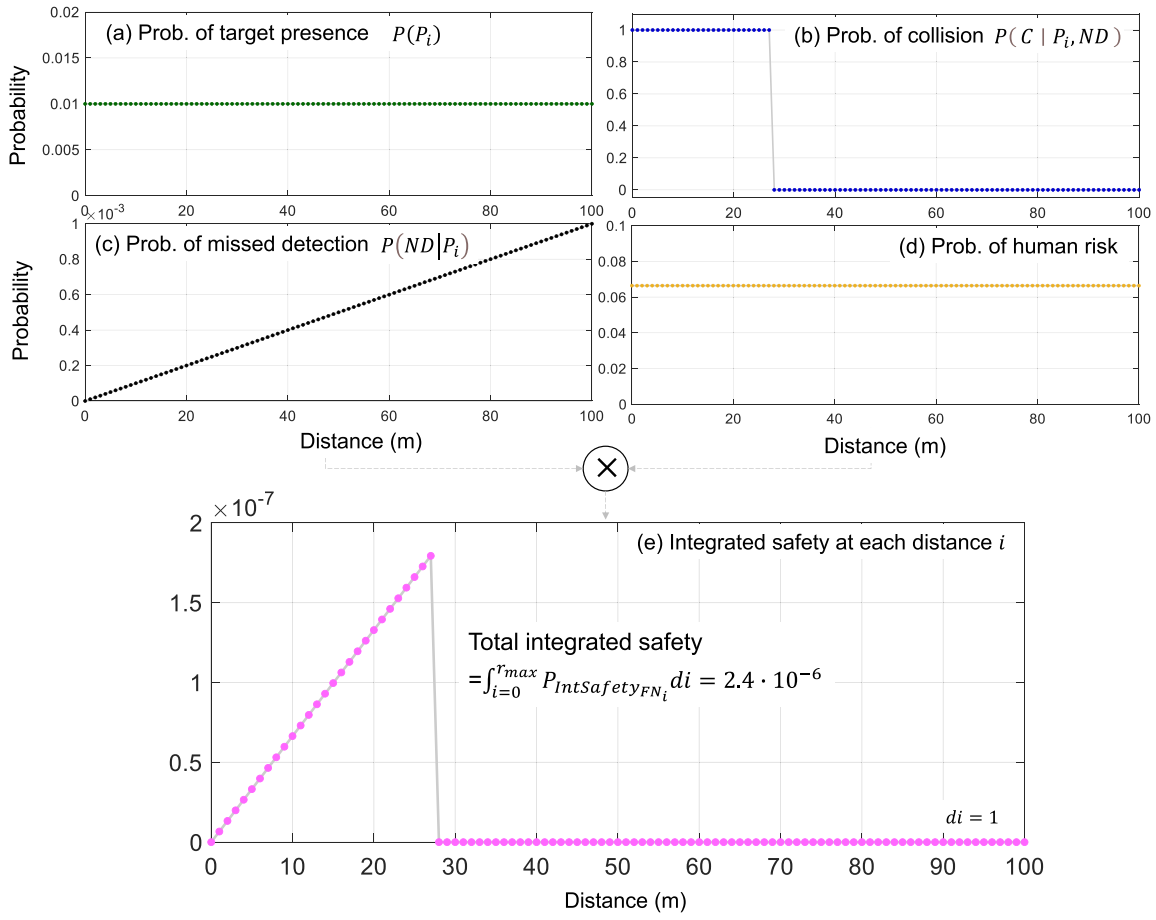

Fig. 10. Simulation of integrated safety risk in FN scenario.

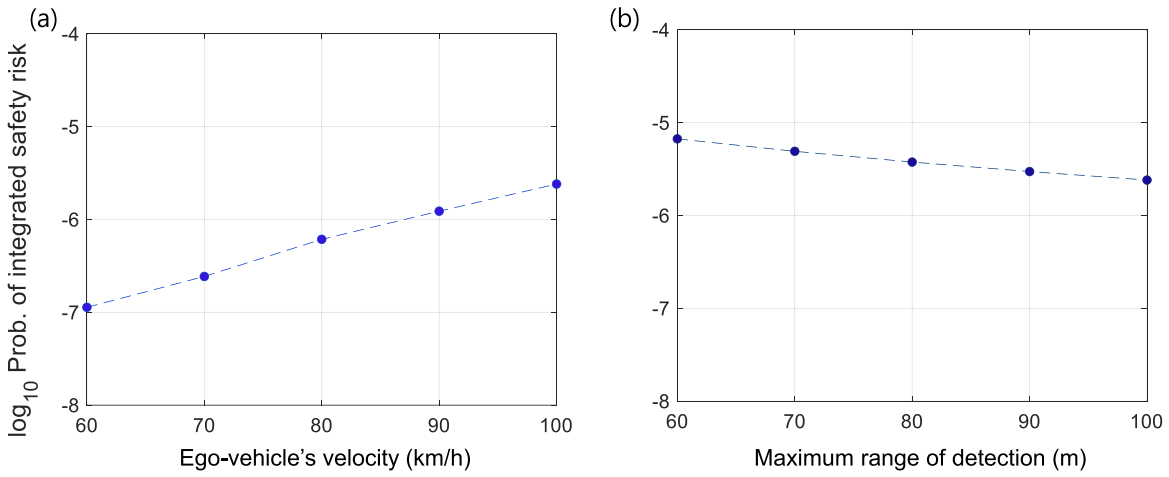

Fig. 11. Sensitivity analysis for FN scenarios as a function of the ego-vehicle's velocity (left) and the maximum range of sensor's detection (right).

any deceleration related to detection. Thus, it can be observed that human injury risk is calculated based on assumed constant ego-vehicle speeds at each possible collision point, resulting in a consistent calculation. Finally, the integrated safety at each distance i is illustrated in Fig. 10(e), and the total integrated safety is the integration of the risk for every i, resulting in $2.4 \bullet 10^{-6}$.

3.4. . Sensitivity analysis for FN scenario

Fig. 11 shows the risks depending on the ego-vehicle's velocity (Fig. 11(a)) and the maximum detection ranges of a sensor (Fig. 11(b)) for a target not detected condition. The results demonstrate a tendency for the safety risk to increase as the ego-vehicle's velocity increases and the maximum detection range decreases. By considering both parameters together, the safety risk can be managed during an operation against either false negatives (FN) or limited detection range scenarios.

3.5. . Demonstration for use-case scenarios

This section aims to present use-cases of the proposed method. Two

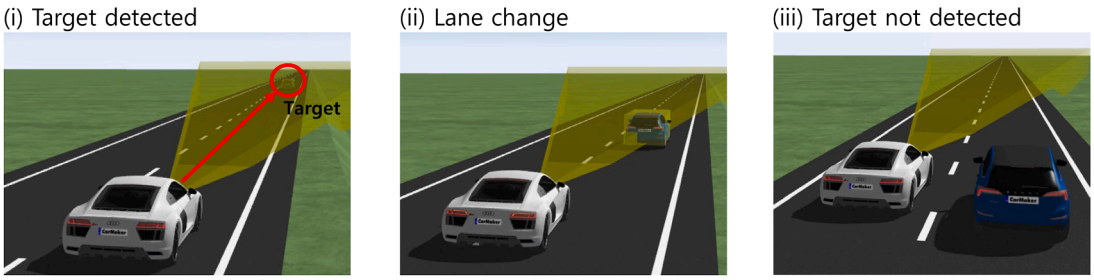

Fig. 12. Simulation scenario performed with the Carmaker simulator [17], where a target vehicle is detected.

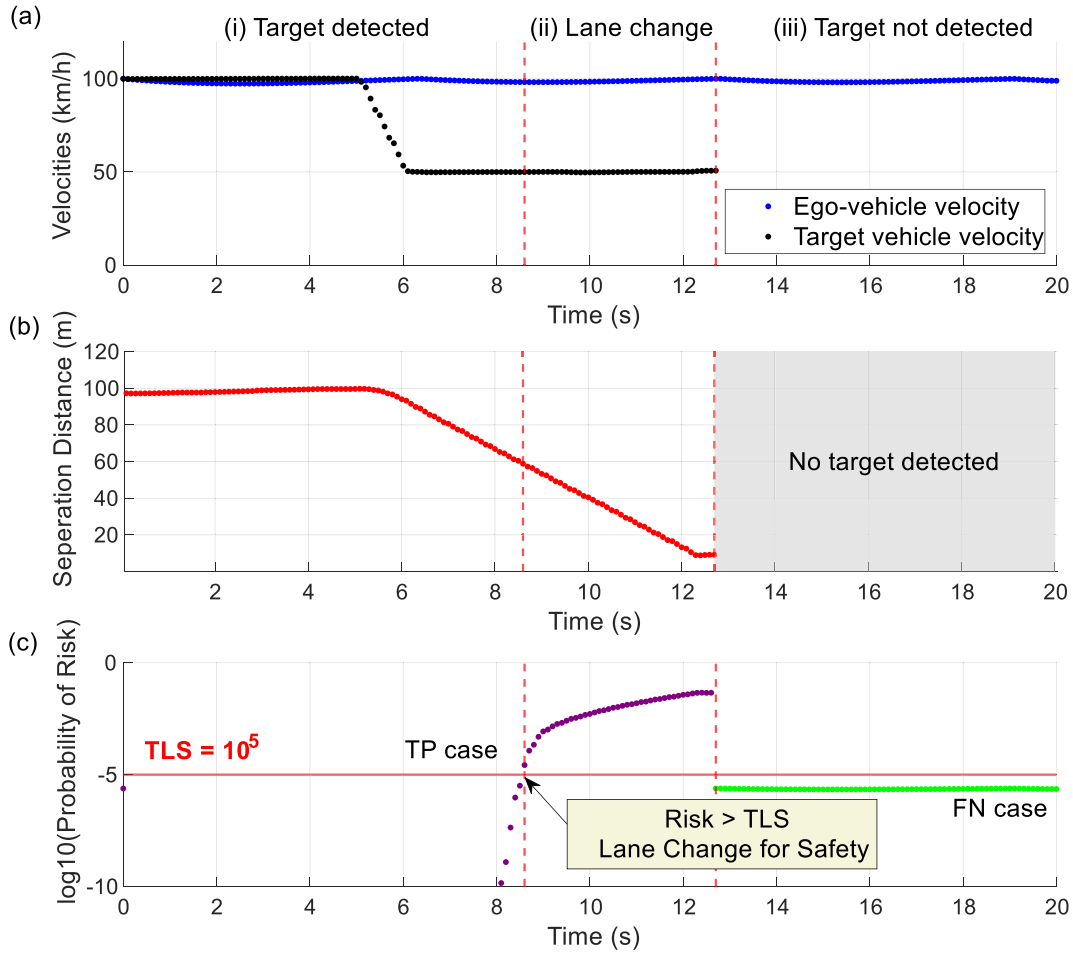

Fig. 13. Results of the use-case simulations for a single target scenario. Vehicle velocities (a), separation distances from the ego-vehicle to the target (b), and the corresponding integrated safety risk (c) are shown as time series.

use-case scenarios are demonstrated: one involves a single target vehicle in the same lane as the ego-vehicle, and the other features two target vehicles–one in the same lane as the ego-vehicle and the other in the left lane. The driving simulator Carmaker, developed by IPG Automotive [17], is used to formulate driving scenarios and obtain simulated data required for risk quantification. In this study, an FCA scenario is modeled in which the ego-vehicle is equipped with a perception sensor with a maximum range of 100 m.

Fig. 12 provides a visual representation of the first simulation scenarios. The simulation begins with the ego-vehicle following a target vehicle. Fig. 12(i) illustrates the detection of the target vehicle. After 5 s, the target vehicle begins to decelerate sharply. When the integrated safety risk value exceeds the target level of safety (TLS) of 10^{-5}, an overtaking maneuver is performed. Fig. 12(ii) shows the execution of this overtaking maneuver. Fig. 12 (iii) then shows the point at which the ego-vehicle passes the target vehicle, after which the perception sensors no longer detect a target vehicle.

Fig. 13 shows the results of the use-case simulations. Fig. 13(a) shows the speeds of the ego-vehicle and the target vehicle. At the beginning of the simulation, both the ego-vehicle and the target vehicle are operating in the same lane, with the ego-vehicle detecting the target. As the target vehicle decelerates after 5 s, the separation distance between the two vehicles, shown in Fig. 13(b), decreases. This decreased separation distance increases the probability of an integrated safety risk, as depicted in Fig. 13(c). In this situation, the ego-vehicle calculates its risk based on the equation defined for the TP condition. When the risk exceeds the TLS of 10^{-5}, the ego-vehicle changes lanes to avoid the target in front, thus maintaining its safety. When the target vehicle is no longer

Fig. 14. Simulation scenario performed with the Carmaker simulator [17], where two target vehicles are detected.

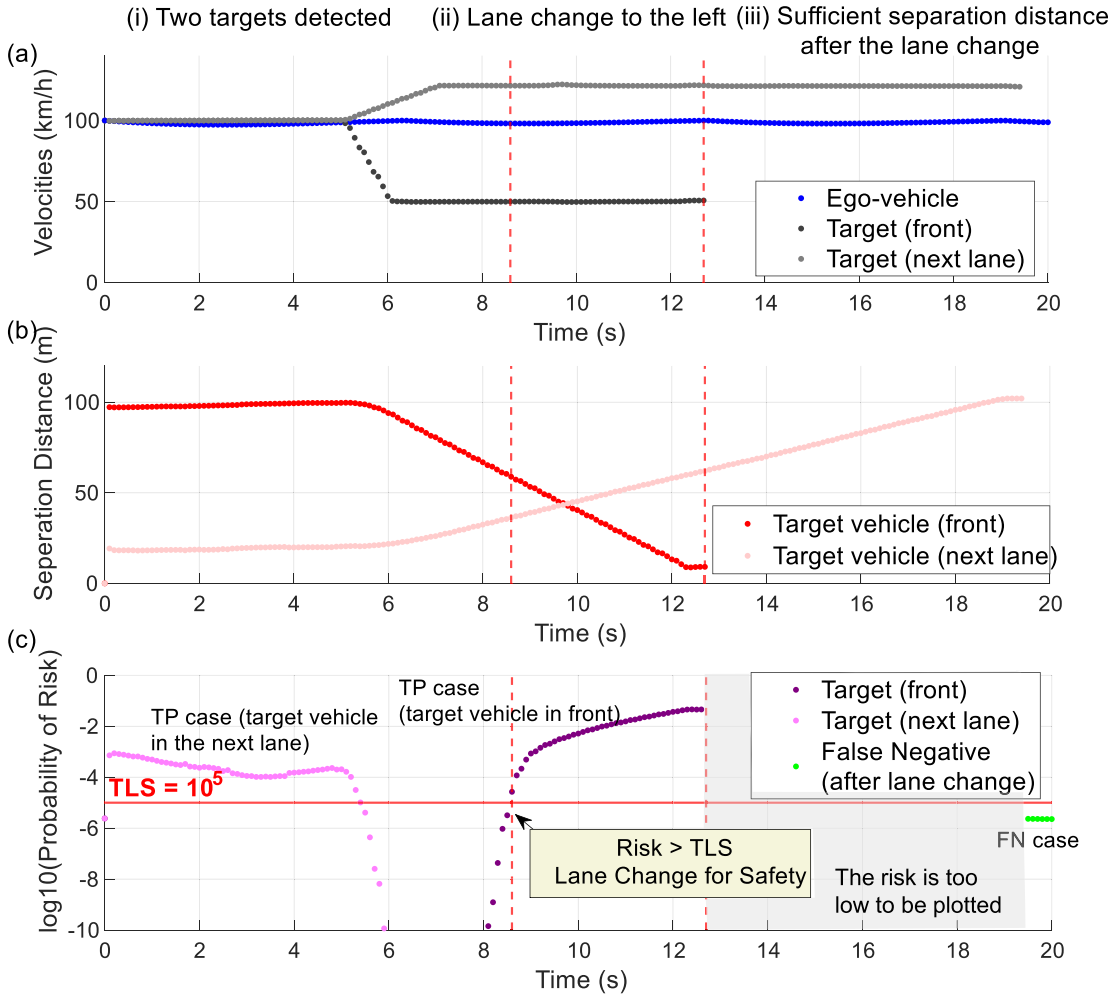

Fig. 15. Results of the use-case simulations for a two-target scenario. Vehicle velocities (a), separation distances from the ego-vehicle to the targets (b), and the corresponding integrated safety risk (c) are shown as time series.

detected, the safety risk is then calculated using the equation defined for the FN situation. After the maneuver, the calculated safety risk level falls below the TLS. This use-case demonstrates the proposed algorithm in action. The transition from the TP case to the FN case, when the target vehicle is no longer detected, highlights the algorithm's capability to handle different hypothesized scenarios.

The use-case is further expanded with the addition of another target vehicle. The secondary target vehicle starts of in the overtaking lane, blocking the possibility of a lane change. The target vehicle in the next lane then accelerates, allowing for a potential lane change. The risks associated with each target vehicle are continuously tracked. Fig. 14 illustrates the events of the simulation for this analysis.

Fig. 15 presents the results of the use-case simulations for a two-target scenario. Fig. 15(a) displays the velocities of the ego-vehicle and both target vehicles. As the target vehicle in the next lane accelerates away, the separation distance from the ego-vehicle increases, as shown in Fig. 15(b). This results in a significant drop in risk, as illustrated by the pink curve in Fig. 15(c). Meanwhile, the target vehicle in front of the ego-vehicle decelerates sharply, causing an increase in its risk. Fig. 15(c) depicts the integrated safety risk for both target vehicles in the scene. Initially, the risk of the target vehicle in the left lane exceeds the TLS, which is assumed to be 10^{-5}, making an overtaking maneuver unsafe. However, as the vehicle accelerates away, its risk drops below the TLS, creating an opportunity for a safe overtake.

Consequently, when the target vehicle in front of the ego-vehicle suddenly brakes, an evasive overtaking maneuver is executed. Again, the maneuver is performed when the risk of the target vehicle in front exceeds the TLS. After the lane change maneuver is completed, the safety risk becomes very low due to sufficient separation distance from the target vehicle in the changed lane, making the risk too low to be plotted. The situation transitions from TP to FN after 19.5 s when the target vehicle is no longer detected. This use case further demonstrates the proposed algorithm in action, tracking risk from multiple target vehicles simultaneously. The simple scenarios illustrated in this section highlight the algorithm's potential as a risk indicator for decision-making and trajectory planning in AVs.

4. Conclusions

This study introduces an innovative methodology for quantifying the integrated safety of AVs under perception sensor uncertainties through a comprehensive probabilistic framework. By subdividing risks based on varying distances to the target and considering both target presence and absence scenarios, the developed algorithm effectively addresses different risks for all possible target locations under detection uncertainty. Simulations for TP and FN scenarios under an FCA scenario illustrate the impact of detection uncertainties, separation distances, vehicle speeds, and sensor ranges on safety risks. Sensitivity analyses show that safety risk increases with higher detection uncertainties and closer separation distances in TP scenarios, and with higher vehicle speeds and shorter detection ranges in FN scenarios. Practical Applications: The proposed framework offers practical insights into regulating separation distances, vehicle speeds, and sensor specifications to enhance AV safety. These findings provide a foundation for future regulatory guidelines and technological advancements aimed at ensuring the safe deployment of AVs. Future Works: This paper focused on demonstrating the framework for calculating integrated safety using a straightforward FCA scenario with a single sensor and either one or two target vehicles. However, the proposed algorithm can be extended to address higher levels of automation in scenarios involving dynamic driving situations, multiple sensors, or interactions with multiple vehicles. Such extensions require careful consideration. For instance, employing a multi-sensor system for risk analysis would necessitate applying the specific characteristics of each sensor type and accounting for variations in parameters defined in our analysis, such as missed detection probability and differing sensor coverage. Additionally, the proposed algorithm can be applied to scenarios involving multiple target vehicles, enabling parallel assessments of safety in multi-target scenarios. Future work will build on this foundation to explore scenarios at higher level of automation.

Funding

This work was supported by the German academic exchange service (DAAD).

CRediT authorship contribution statement

Jinsil Lee: Writing – original draft, Visualization, Validation, Software, Methodology, Investigation, Data curation, Conceptualization. **Mel Vincent Dela Cruz:** Writing – review & editing, Visualization, Validation, Software, Methodology, Investigation, Data curation. **Ralf Sturm:** Writing – review & editing, Supervision, Project administration, Methodology, Conceptualization.

Declaration of competing interest

None.

Data availability

Data will be made available on request.

References

[1] M. Berk. Safety assessment of environment perception in automated driving vehicles, doctoral dissertation, Technische Universität München, 2019.
[2] M. Berk, O. Schubert, H.M. Kroll, B. Buschardt, D. Straub, Exploiting redundancy for reliability analysis of sensor perception in automated driving vehicles, IEEE Trans. Intell. Transp. Syst. 21 (2020) 5073–5085, https://doi.org/10.1109/TITS.2019.2948394.
[3] R.M. Brach, Uncertainty in accident reconstruction calculations, SAE Tech. Pap. 103 (1994) 909–916, https://doi.org/10.4271/940722.
[4] F. Char, T. Serre, Analysis of pre-crash characteristics of passenger car to cyclist accidents for the development of advanced drivers assistance systems, Accid. Anal. Prev. 136 (2020) 105408, https://doi.org/10.1016/j.aap.2019.105408.
[5] J. Cui, G. Sabaliauskaite, L.S. Liew, F. Zhou, B. Zhang, Collaborative analysis framework of safety and security for autonomous vehicles, IEEE Access 7 (2019) 148672–148683, https://doi.org/10.1109/ACCESS.2019.2946632.
[6] F. de Ponte Müller, Survey on ranging sensors and cooperative techniques for relative positioning of vehicles, Sensors 17 (2017) 1–27, https://doi.org/10.3390/s17020271 (Switzerland).
[7] Desmond Yuen, 2021. Can you react faster than a self-driving car on 5G networks? [WWW Document]. URL https://medium.com/predict/making-roads-safer-with-self-driving-cars-and-5g-c1e28526362c.
[8] T. Dirndorfer, M. Botsch, Model-based analysis of sensor-noise in predictive passive safety algorithms, in: Proceedings of the 22nd International Technical Conference on the Enhanced Safety of Vehicles (ESV), 2011.
[9] S.D. Doecke, M.R.J. Baldock, C.N. Kloeden, J.K. Dutschke, Impact peed and the risk of serious injury in vehicle crashes, Accid. Anal. Prev. 144 (2020) 105629, https://doi.org/10.1016/j.aap.2020.105629.
[10] C. Fu, Z. Lu, N. Ding, W. Bai, Distance headway-based safety evaluation of emerging mixed traffic flow under snowy weather, Physica A 642 (2024) 129792, https://doi.org/10.1016/j.physa.2024.129792.
[11] C. Greer, E. Griffor, D. Wollman, Workshop Report : Consensus Safety Measurement Methodologies for Automated Driving System-Equipped Vehicles, U. S. Department of Commerce, 2019, p. 20.
[12] B. Grotz, P. Straßburger, A. Huf, L. Roig, Predictive safety-perception-based activation of pre-crash systems, ATZ Worldw. 123 (2021) 18–25.
[13] M. Guzek, Z. Lozia, Computing methods in the analysis of road accident reconstruction uncertainty, Arch. Comput. Methods Eng. 28 (2021) 2459–2476, https://doi.org/10.1007/s11831-020-09462-w.
[14] C.M. Hruschka, D. Töpfer, S. Zug, Risk assessment for integral safety in automated driving, in: Proceedings of the 2019 2nd International Conference on Intelligent Autonomous Systems, ICoIAS, 2019, https://doi.org/10.1109/ICoIAS.2019.00025, 2019 102–109.
[15] ICAO, 2018. Annex 10–Aeronautical telecommunications. International standards and recommended practices 1.
[16] ICAO, 2003. The guidance material on the implementation of a 300 m (1000 ft) vertical separation minimum.
[17] IPG-Automotive, Driving Simulator, Carmaker, 2024.
[18] ITU-R, 2015. Systems characteristics and compatibility of automotive radars operating in the frequency band 77.5-78 GHz for sharing studies 0.
[19] Jerhot, J., Stanek, G., Meinecke, M.M., Knaup, J., 2009. Integrated probabilistic approach to environmental perception with self-diagnosis capability for advanced driver assistance systems.
[20] M. Joerger, G. Duenas Arana, M. Spenko, B. Pervan, A new approach to unwanted-object detection in GNSS/LiDAR-based navigation, Sensors 18 (2018), https://doi.org/10.3390/s18082740 (Switzerland).
[21] C. Katrakazas, M. Quddus, W.H. Chen, A new integrated collision risk assessment methodology for autonomous vehicles, Accid. Anal. Prev. 127 (2019) 61–79, https://doi.org/10.1016/j.aap.2019.01.029.
[22] J. Khoury, K. Amine, R. Abi Saad, An initial investigation of the effects of a fully automated vehicle fleet on geometric design, J. Adv. Transp. 2019 (2019), https://doi.org/10.1155/2019/6126408.
[23] Kusano, K.D., Scanlon, J.M., Chen, Y.H., McMurry, T.L., Chen, R., Gode, T., Victor, T., 2023. Comparison of Waymo rider-only crash data to human benchmarks at 7.1 million miles. arXiv preprint arXiv:2312.12675.
[24] J. Lee, J. Lee, Correlation between ionospheric spatial decorrelation and space weather intensity for safety-critical differential GNSS systems, Sensors 19 (2019), https://doi.org/10.3390/s19092127 (Switzerland).
[25] Jinsil Lee, S. Pullen, S. Datta-Barua, J. Lee, Real-time ionospheric threat adaptation using a space weather prediction for GNSS-based aircraft landing systems, IEEE Trans. Intell. Transp. Syst. 18 (2017) 1752–1761, https://doi.org/10.1109/TITS.2016.2627600.
[26] J. Lenard, R. Welsh, R. Danton, Time-to-collision analysis of pedestrian and pedal-cycle accidents for the development of autonomous emergency braking systems, Accid. Anal. Prev. 115 (2018) 128–136, https://doi.org/10.1016/j.aap.2018.02.028.
[27] T.J. Leung, J. Rife, Refining fault trees using aviation definitions for consequence severity, IEEE Aerosp. Electron. Syst. Mag. 32 (2017) 4–14, https://doi.org/10.1109/MAES.2017.150171.

[28] S. Magdici, M. Althoff, Adaptive cruise control with safety guarantees for autonomous vehicles, IFAC-PapersOnLine 50 (2017) 5774–5781, https://doi.org/10.1016/j.ifacol.2017.08.418.
[29] E. Martí, M.Á. de Miguel, F. García, J. Pérez, A review of sensor technologies for perception in automated driving, IEEE Intell. Transp. Syst. Mag. 11 (2019) 94–108, https://doi.org/10.1109/MITS.2019.2907630.
[30] Mercedes-Benz Group, 2024. Certification for SAE level 3 system for U.S. market [WWW Document]. https://group.mercedes-benz.com/innovation/product-innovation/autonomous-driving/drive-pilot-nevada.html.
[31] A.S. Mueller, J.B. Cicchino, D.S. Zuby, What humanlike errors do autonomous vehicles need to avoid to maximize safety? J. Saf. Res. 75 (2020) 310–318, https://doi.org/10.1016/J.JSR.2020.10.005.
[32] F.D.P. Muller, E.M. Diaz, I. Rashdan, Cooperative positioning and radar sensor fusion for relative localization of vehicles, in: Proceedings of the IEEE Intelligent Vehicles Symposium, 2016, pp. 1060–1065, https://doi.org/10.1109/IVS.2016.7535520, 2016-Augus.
[33] S. Pullen, J. Kilfeather, J. Goddard, T. Nowitzky, B. Shah, W. Doong, A. Welton, D. Kagan, K. Greer, Enhanced navigation, robustness, and safety assurance for autonomous vehicles as part of the Globalstar connected car program, in: Proceedings of the 31st International Technical Meeting of the Satellite Division of the Institute of Navigation, 2018, pp. 1538–1565, https://doi.org/10.33012/2018.16106. ION GNSS+ 2018.
[34] M.T. Rahman, K. Dey, V. Dimitra Pyrialakou, S. Das, Factors influencing safety perceptions of sharing roadways with autonomous vehicles among vulnerable roadway users, J. Saf. Res. 85 (2023) 266–277, https://doi.org/10.1016/J.JSR.2023.02.010.
[35] T.G.R. Reid, S.E. Houts, R. Cammarata, G. Mills, S. Agarwal, A. Vora, G. Pandey, Localization requirements for autonomous vehicles, SAE Int. J. Connect. Autom. Veh. (2019), https://doi.org/10.4271/12-02-03-0012.
[36] A. Reschka, J.R. Böhmer, F. Saust, B. Lichte, M. Maurer, Safe, dynamic and comfortable longitudinal control for an autonomous vehicle, in: Proceedings of the IEEE Intelligent Vehicles Symposium, Proceedings, 2012, pp. 346–351, https://doi.org/10.1109/IVS.2012.6232159.
[37] Roturier, B., Chatre, E., Ventura-Traveset, J., 2001. The SBAS integrity concept standardised by ICAO-application to EGNOS. NAVIGATION-PARIS- 49, 65–77.
[38] RTCA, 2004. Minimum aviation system performance standards for the local area augmentation system (LAAS).
[39] SAE International, 2018. Surface vehicle recommended practice: taxonomy and definitions for terms related to driving automation systems for on-road motor vehicles (J3016B).
[40] J.M. Scanlon, K.D. Kusano, T. Daniel, C. Alderson, A. Ogle, T. Victor, Waymo simulated driving behavior in reconstructed fatal crashes within an autonomous vehicle operating domain, Accid. Anal. Prev. 163 (2021) 1–16, https://doi.org/10.1016/j.aap.2021.106454.
[41] Shalev-Shwartz, S., Shammah, S., Shashua, A., 2017. On a formal model of safe and scalable self-driving cars. ArXiv 1–37.
[42] E.R. Teoh, D.G. Kidd, Rage against the machine? Google's self-driving cars versus human drivers, J. Saf. Res. 63 (2017) 57–60, https://doi.org/10.1016/j.jsr.2017.08.008.
[43] C. Urmson, Driving beyond stopping distance constraints, in: Proceedings of the IEEE/RSJ International Conference on Intelligent Robots and Systems, IEEE, 2006, pp. 1189–1194.
[44] Z. Wang, Y. Wu, Q. Niu, Multi-sensor fusion in automated driving: a survey, IEEE Access 8 (2020) 2847–2868, https://doi.org/10.1109/ACCESS.2019.2962554.
[45] C. Wang, Y. Xie, H. Huang, P. Liu, A review of surrogate safety measures and their applications in connected and automated vehicles safety modeling, Accid. Anal. Prev. 157 (2021) 106157, https://doi.org/10.1016/j.aap.2021.106157.
[46] Wishart, J., Como, S., Elli, M., Russo, B., Weast, J., Altekar, N., James, E., 2020. Driving safety performance assessment metrics for ADS-equipped vehicles. SAE Technical Papers 2020-April, 2881–2899. 10.4271/2020-01-1206.
[47] E. Yurtsever, J. Lambert, A. Carballo, K. Takeda, A survey of autonomous driving: common practices and emerging technologies, IEEE Access 8 (2020) 58443–58469, https://doi.org/10.1109/ACCESS.2020.2983149.
[48] T. Zhou, M. Yang, K. Jiang, H. Wong, D. Yang, Mmw radar-based technologies in autonomous driving: a review, Sensors (2020), https://doi.org/10.3390/s20247283 (Switzerland).

Jinsil Lee received her B.S. degree in civil and environmental engineering, and Ph.D. degree in aerospace Engineering from Korea Advanced Institute of Science and Technology (KAIST) in 2012, and 2019, respectively. She is currently working as a senior researcher at the Korea Aerospace Research Institute (KARI, jinsil@kari.re.kr). Prior to her current position, she was a researcher in the institute of vehicle concepts at the German Aerospace Center (DLR). Her research interests include developing sensor systems for navigation and perception of autonomous vehicles and methodologies to ensure integrated safety of future mobility systems to support the high level of automation.

Mel Vincent Dela Cruz completed his studies Bachelor's Degree in Aeronautical Engineering in the University of Limerick, Ireland where he wrote his thesis on Planar Vibrational Energy Harvesting. In 2019, Mel completed an internship in DLR on structural optimization and numerical surrogate models. He then participated in a semester abroad in Georgia Institute of Technology (USA) where he furthered his engineering knowledge. Mel is currently pursuing hid PhD in the "Integrated Safety of Autonomous Vehicles" as part of a collaboration between DLR and Coventry University, UK.

Ralf Sturm studied from the aerospace engineering department at the university of Stuttgart. He worked at the DLR institute of structure and design in the field of crashworthiness of aircraft. After his Ph.D. in the corresponding research field, he changed to the DLR institute of the vehicle concept. Currently, Ralf Sturm is the team leader "Structural Optimization and Integrated Safety" group in the "Vehicle Architectures and Lightweight Design Concepts". The main focus of the group is the development of the method for both active and passive safety to ensure the safety of future vehicles.